ACS APPLIED MATERIALS & INTERFACES

Research Article

www.acsami.org

Design of Hybrid Nanostructural Arrays to Manipulate SERS-Active Substrates by Nanosphere Lithography

Xiaoyu Zhao,[†,‡] Jiahong Wen,[†,‡] Mengning Zhang,[§] Dunhui Wang,*[,†,‡] Yaxin Wang,[§] Lei Chen,[§] Yongjun Zhang,*[,§] Jinghai Yang,[§,∥] and Youwei Du[†,‡]

[†]National Laboratory of Solid State Microstructures and Jiangsu Key Laboratory for Nanotechnology and [‡]Collaborative Innovation Center of Advanced Microstructures, Nanjing University, Nanjing 210093, PR China

[§]Key Laboratory of Functional Materials Physics and Chemistry, Jilin Normal University, Ministry of Education, Siping 136000, PR China

[∥]Changchun Institute of Optics, Fine Mechanics and Physics, Chinese Academy of Sciences, Changchun 130033, PR China

ABSTRACT: An easy-handling and low-cost method is utilized to controllably fabricate nanopattern arrays as the surface-enhanced Raman scattering (SERS) active substrates with high density of SERS-active areas (hot spots). A hybrid silver array of nanocaps and nanotriangles are prepared by combining magnetron sputtering and plasma etching. By adjusting the etching time of polystyrene (PS) colloid spheres array in silver nanobowls, the morphology of the arrays can be easily manipulated to control the formation and distribution of hot spots. The experimental results show that the hybrid nanostructural arrays have large enhancement factor, which is estimated to be seven times larger than that in the array of nanocaps and three times larger than that in the array of nanorings and nanoparticles. According to the results of finite-difference time-domain simulation, the excellent SERS performance of this array is ascribed to the high density of hot spots and enhanced electromagnetic field.

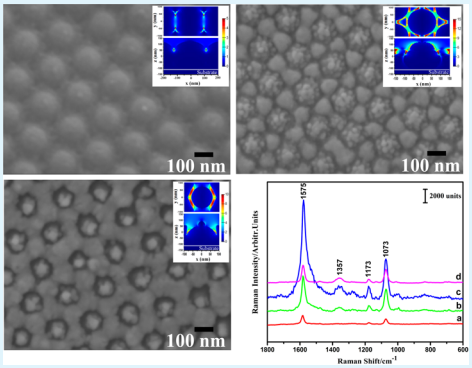

KEYWORDS: *surface-enhanced Raman scattering (SERS), nanostructrual arrays, silver film, nanosphere lithography (NSL), hot spots*

1. INTRODUCTION

Surface enhanced Raman scattering (SERS) is the most promising spectroscopy technique for biochemistry,[1,2] chemical detection,[3] surface science,[4,5] and so on since it is non-destructive, ultrasensitive, and selective.[1] It is known that the SERS substrate with high density of SERS-active areas (hot spots) is greatly desired since it can achieve enhanced Raman signals.[6] Accordingly, many studies about SERS are focused on the preparation of substrates with noble metal nanoparticles and ordered nanostructural arrays with nanogaps,[6] which can provide hot spots with enhanced electromagnetic field. However, during the preparation of these SERS substrates, the aggregation of metal nanoparticles will lead to the reduced density and inhomogeneous distribution of the hot spots, which remarkably decrease the enhancement factor (EF).[7−10] Therefore, the preparation of SERS substrates with large area and high density of hot spots remains a great challenge. It is reported that the low-cost nanosphere lithography (NSL) is an important method to prepare SERS-active substrates.[3,4,6] Through this method, a wide variety of nanopatterns with large areas such as periodic nanocaps,[11−14] nanotriangles,[15−17] nanobowls,[18,19] nanotubes, nanorings,[20,21] and nanopillars arrays[22] can be prepared. More importantly, many nanogaps can be formed in these nanostructural arrays by adjusting the technical parameters.[11−22] Consequently, the density of hot spots can be significantly improved in the SERS substrates prepared by NSL.[6,11,15]

Generally, a monolayer of close-packed polystyrene (PS) colloid spheres array is used as a template for the preparation of large-area and ordered nanostructrual arrays by NSL. When some metals are deposited on the template by evaporating or sputtering, two different kinds of nanostructural arrays are generated. One is the hexagonally regular array of metal film over nanosphere, and the other is the nanotriangles array which is formed after the removal of the template.[16,22,23] Here the noble metal is usually utilized to deposit on the template since it can generate localized surface plasmon resonance (LSPR) which is helpful to obtain the enhanced electromagnetic field.[24] It is worth noting that using the technology of NSL hot spots of nanostructural arrays can be manipulated by adjusting the preparing parameters which is promising with regard to achieving enhanced SERS signals.[12,17] By combining the technologies of magnetron sputtering and plasma etching, an easy-handling and low-cost method is proposed in this paper to fabricate a hybrid nanostructural array, which is composed of nanocaps and nanotriangles. Through this method, the formation and distribution of hot spots can be easily

Received: November 2, 2016
Accepted: February 13, 2017
Published: February 13, 2017

DOI: 10.1021/acsami.6b14008
ACS Appl. Mater. Interfaces 2017, 9, 7710−7716

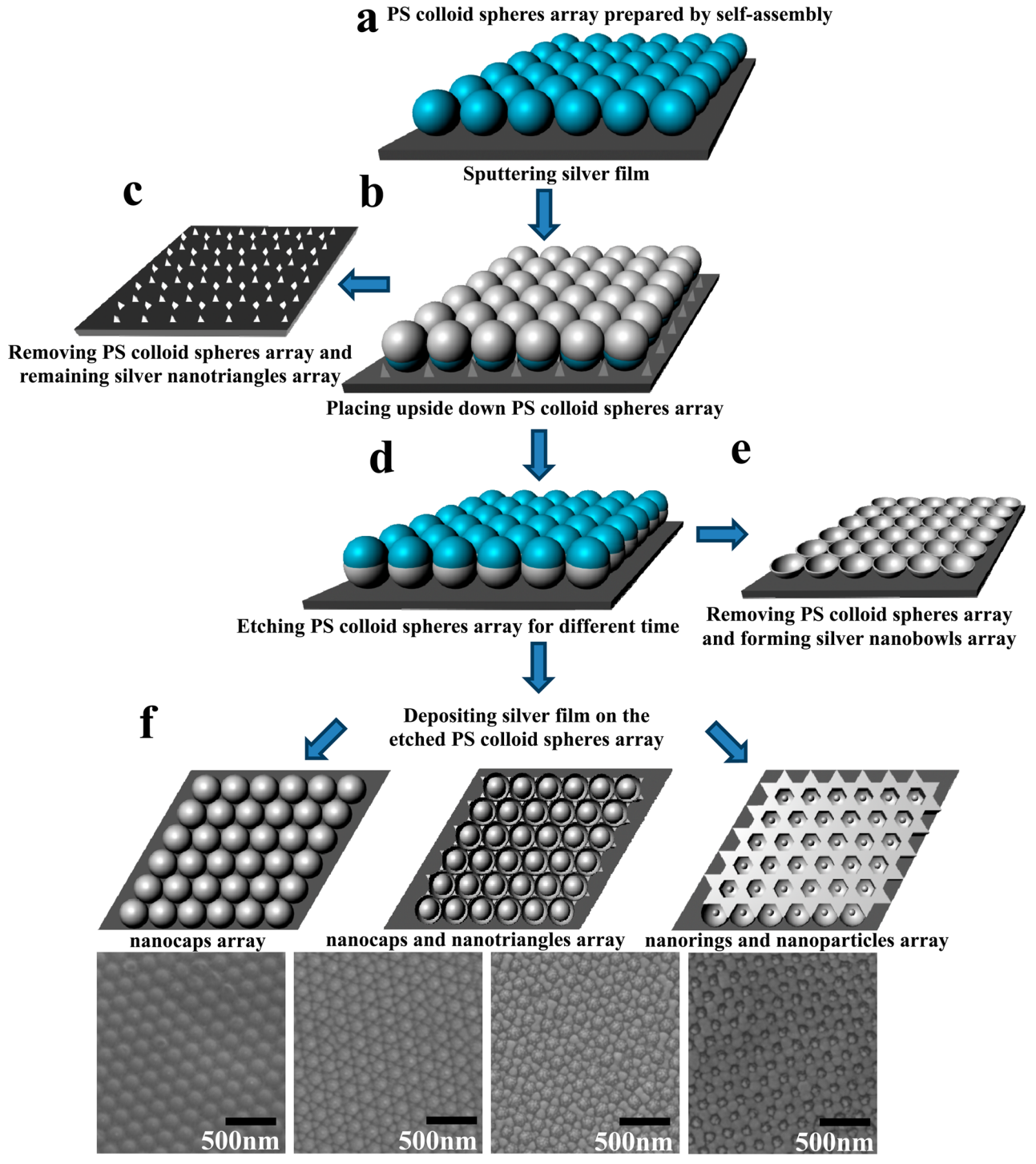

Figure 1. Schematic of preparation of the silver nanostructural arrays.

manipulated to control the morphology of nanostructural arrays, which significantly increase the density of hot spots. The results of finite-difference time-domain (FDTD) simulation demonstrate that large EF in our nanostructural arrays is due to the high density of hot spots and enhanced electromagnetic field.

2. EXPERIMENTAL SECTION

2.1. Preparation of the Large-Area and Ordered PS Colloid Spheres Array. PS colloid spheres with diameter of 200 nm monodispersed in 10 wt % aqueous solution were commercially supplied by Duke corporation. A monolayer array of close-packed PS colloid spheres was fabricated by the self-assembly method on a hydrophilic silicon wafer and the area of the PS colloid spheres array was about 1 cm^2. The self-assembly method was described in detail in our previous work.[25]

2.2. Fabrication of the Silver Nanostructural Arrays. The silver film coated on the PS colloid spheres array was fabricated by using the magnetron sputtering technique (ATC 1800-F, AJA, USA). The base pressure of vacuum chamber was 2.0×10^{-4} Pa. During the film deposition, the distance between the PS colloid spheres array substrate and the silver target was 20 cm. Argon with purity of 99.999% was used as the working gas with a pressure of 0.6 Pa. The silver film was deposited with a rate of 0.17 nm s^{-1}, while the

DOI: 10.1021/acsami.6b14008
ACS Appl. Mater. Interfaces 2017, 9, 7710−7716

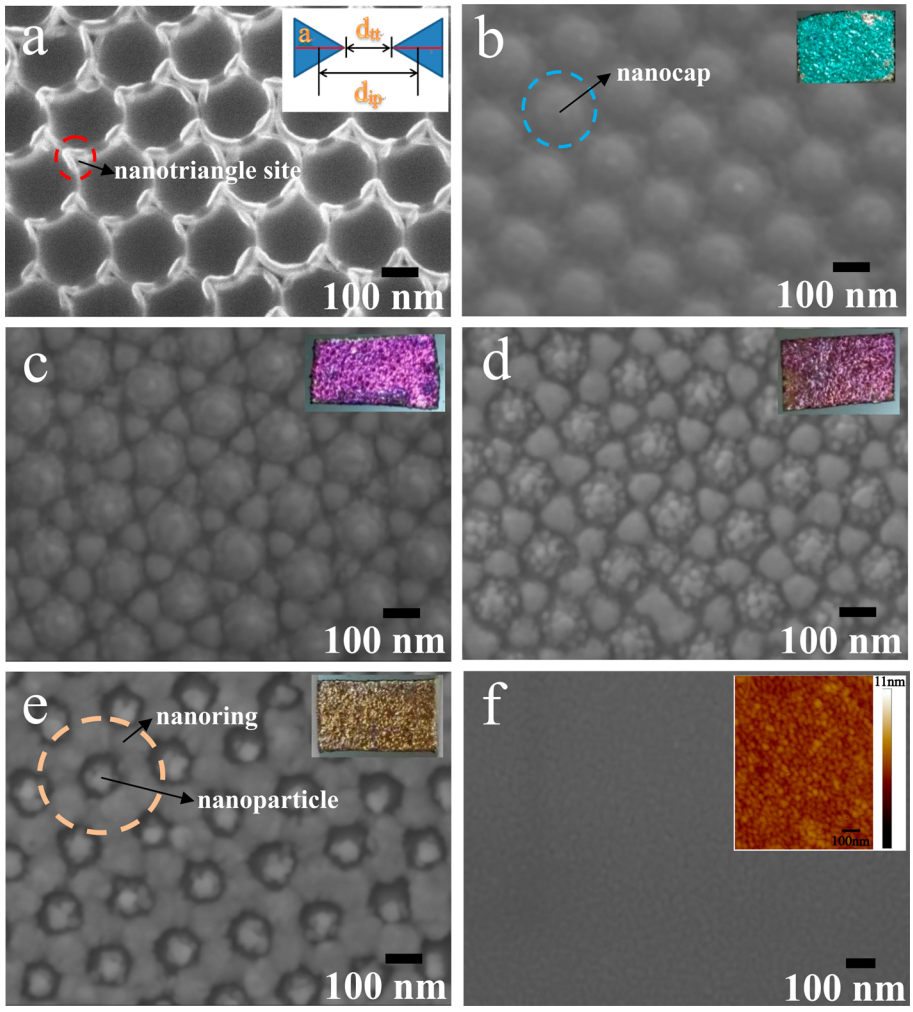

Figure 2. SEM images for (a) the silver nanobowls array; silver film on PS colloid spheres array etched for (b) 0 s, (c) 60 s, (d) 120 s, (e) 240 s, and (f) silver film on silicon wafer. The insets are the schematic image of the neighboring silver nanotriangle sites (a), optical photos of the different nanostructural arrays (b–e), and AFM image of silver film on silicon wafer (f).

sputtering power was 17 W. Afterward, the silver nanocaps array was stripped by 3M double-sided tape from the original silicon wafer and removed upside down to the other silicon wafer immediately. Then, the PS colloid spheres were etched by different time (0, 60, 120, and 240 s) with a rate of 1 nm s^{-1} in a plasma cleaner equipment (Model 1020, E.A. Fischione Instruments Inc.). With the increase of etching time, the diameter of the PS colloid sphere decreased gradually while the shape and periodicity of the PS colloid spheres array kept unchanged.[26] Finally, the silver film of 20 nm was deposited on the etched PS colloid spheres array in the silver nanobowls using the same depositing conditions.

2.3. Characterization of the Silver Nanostructural Arrays. The scanning electron microscopy (SEM) images of the silver nanostructural arrays were recorded by a JEOL 7800F. The reflection spectra were measured by a spectrophotometer (Shimadzu UV-3600).

2.4. SERS Measurements. SERS spectra were measured with the radiation laser of 532 nm using Renishaw Micro-Raman spectrometer.[25] The nanostructural arrays were immersed into the 4-mercaptobenzoic acid (4-MBA) ethanol solution (10^{-3} mol/L) for 30 min. After that, the substrates were washed with anhydrous ethanol and dried with nitrogen gas before SERS measurement.

2.5. FDTD Simulations. The FDTD simulation was performed using commercial software (Lumerical FDTD solution). The substrates were placed in the $x-y$ plane. A unit of the periodic structure along the x, y, and z was simulated.[27] The distribution of electromagnetic field was simulated with a 532 nm laser. The light was normal incidence, and the refractive index of PS colloid sphere was considered to be 1.585. The permittivity and permeability parameters of silver were provided by the software material database.[28] The geometric parameters of the silver nanostructural arrays were obtained from the SEM images.

3. RESULTS AND DISCUSSION

3.1. Fabrication Process and Characterization of the Silver Nanostructural Arrays. Figure 1 presents the preparation process of the silver nanostructrual arrays. First, the ordered PS colloid spheres (200 nm) array is fabricated on a silicon wafer using the self-assembly technique (Figure 1a). Then, silver film is deposited on the close-packed PS colloid spheres array along perpendicular direction, forming a nanocaps array on the ordered PS colloid spheres array. Meanwhile, the silver nanoparticles can penetrate the interstice among the three nearest-neighboring PS colloid spheres to reach the silicon wafer substrate, creating a triangular-shaped silver nanoparticle arrays with *P6mm* symmetry, which is shown in Figure 1b. Then, the close-packed nanocaps array is stripped via 3M double-sided tape from the silicon wafer. As shown in Figure 1c, the silver nanotriangles array is retained on the silicon wafer. After that, the close-packed nanocaps array is removed upside down to the other silicon wafer (Figure 1d). When the close-packed nanocaps array is completely inverted

DOI: 10.1021/acsami.6b14008
ACS Appl. Mater. Interfaces 2017, 9, 7710–7716

and the PS colloid spheres are all removed, a silver nanobowls array is formed which is shown in Figure 1e. Next, the PS colloid spheres in the silver nanobowls are etched with different etching time (0, 60, 120, and 240 s) to form the smaller ones. Finally, the silver film of 20 nm is deposited on the etched PS colloid spheres array in the silver nanobowls using the same depositing conditions. As shown in Figure 1f, three different nanostructural arrays are obtained by this method.

Figure 2a shows the SEM image of the silver nanobowls array in which some nanotriangle sites are observed among the three nearest-neighboring PS colloid spheres. Based on the geometric calculation of the close-packed PS colloid spheres array,[11] the relationship between the nanotriangle spacing (d_{ip}) and the perpendicular bisector of the nanotriangle (a) to PS colloid sphere diameter (D) is expressed as $d_{ip} = \frac{1}{\sqrt{3}}D$ and $a = \frac{3}{2}\left(\sqrt{3} - 1 - \frac{1}{\sqrt{3}}\right)D$. Here the sizes of d_{ip} and a are calculated to be about 115 and 46 nm, respectively. These results agree well with those estimated from the magnified SEM image (d_{ip} = 115 ± 5 nm and a = 46 ± 5 nm). Here the distance between the nearest tips of nanotriangle (d_{tt}) is about 54 ± 5 nm. The schematic image of d_{ip}, a, and d_{tt} is plotted in the inset of Figure 2a.

Figure 2b–e shows the SEM images of three types of the silver nanostructrual arrays. The corresponding optical photos given in the insets show different reflected colors, which are ascribed to the different diameters of PS colloid spheres array. For the same type of silver nanostructrual arrays, the uniform diffraction color indicates that the high-ordered PS colloid spheres array is formed.[26] The formation of these silver nanostructrual arrays are strongly dependent on the etching time of PS colloid spheres array in the silver nanobowls. When the etching time is 0 s, only the nanocaps array is observed. Under this condition, the sizes of unetched PS colloid spheres are large enough,[21] so the nanotriangle sites are too small to be distinguished in Figure 2b. As the etching time increases to 60 s, some nanotriangles with average size of a = 65 ± 5 nm are observed. These nanotriangles and nanocaps compose a hybrid nanostructural array, which is shown in Figure 2c. Between the every two neighboring nanaotriangles, a nanogap with average size of d_{tt} = 34 ± 5 nm is formed. Besides these nanogaps, another type of nanogap which locates between the neighboring nanocaps and nanotriangles are observed as well. However, due to the relatively large size of the nanocaps, this type of nanogap is very narrow, and the number of them is limited. When the etching time is 120 s, the morphology of the nanostructural array is not changed, but the size of nanocaps further decreases, forming a larger nanotriangle with the average size of a = 85 ± 5 nm. Due to the reduced size of PS colloid spheres, the surface of nanocaps with silver nanoparticles becomes rough. Under this condition, the nanogaps between nanocaps and nanotriangles enlarge, and the number of these nanogaps increases remarkably. Meanwhile, the average size of nanogap between the every two neighboring nanaotriangles d_{tt} decreases to 14 ± 5 nm, which is shown in Figure 2d. When the etching time increases to 240 s, the PS colloid spheres are etched away completely. At this time, all adjacent nanotriangles connect to each other, and the size of d_{tt} decreases to almost zero. Now, a new nanostructural array of nanorings and nanoparticles is formed, which can be observed from Figure 2e. In this array, the nanogaps only locate between the nanorings and nanoparticles, leading to the decreased number of nanogaps. The silver film is also deposited on the silicon wafer, which is shown in Figure 2f. As estimated from the inset, the average size of silver nanoparticle is about 25 nm, which will be used in the following FDTD simulation.

3.2. Evaluation of SERS Activity of the Silver Nanostructural Arrays. In order to select the proper exciting light wavelength in SERS measurement, the reflection spectra of three types of silver nanostructrual arrays are measured. As shown in Figure 3, two localized surface plasmon resonance

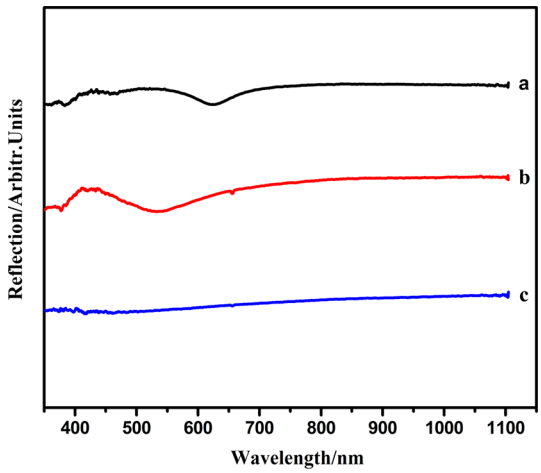

Figure 3. Reflection spectra of three types of silver nanostructural arrays. (a) nanocaps array, (b) nanocaps and nanotriangles array (etched for 120 s), and (c) nanorings and nanoparticles array.

(LSPR) bands are observed at 622 and 525 nm, for the array of nanocaps and the array of nanocaps and nanotriangles (etched for 120 s), respectively. For the array of nanorings and nanoparticles, no obvious LSPR band is observed. Thus, we select the 532 nm laser as an excitation light to match LSPR band in SERS measurement.

Figure 4 shows the typical SERS spectra of the silver nanostructrual arrays, in which 4-MBA is used as a SERS probe. Two strong SERS peaks appearing at about 1575 and 1073

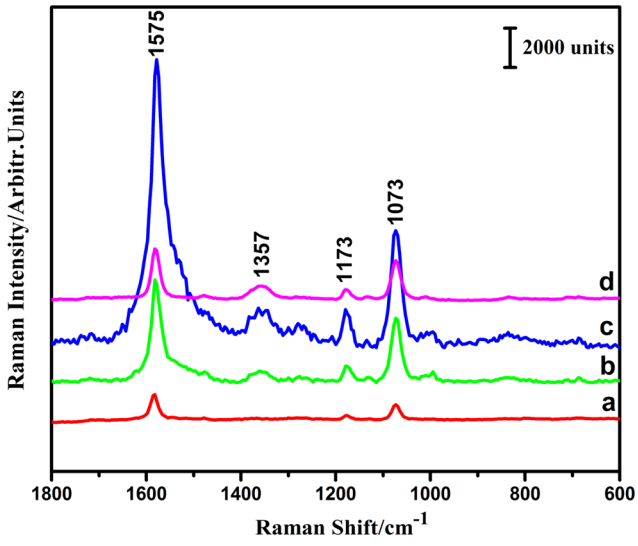

Figure 4. Raman spectrum of 4-MBA for silver film on PS colloid spheres array etched for (a) 0 s, (b) 60 s, (c) 120 s, and (d) 240 s, under 532 nm laser excitation.

DOI: 10.1021/acsami.6b14008
ACS Appl. Mater. Interfaces 2017, 9, 7710–7716

cm^{-1} are assigned to aromatic ring vibrations, which are employed to evaluate the SERS activity of different substrates. The weaker SERS peaks at about 1173 and 1357 cm^{-1} are assigned to the C−H deformation and COO^- stretching vibration modes, respectively.[29−32] For the silver nanostructural arrays, the SERS intensity of 4-MBA first increases with the increasing etching time and shows the highest enhancement at 120 s. When the etching time increases to 240 s, a remarkable decrease of the SERS signals is observed. It is well-known that the SERS signals is closely related to the electromagnetic field derived from the LSPR effect of noble metals.[24] In the nanostructural SERS substrates, the hot spot located at the nanogaps can lead to the further enhancement of the electromagnetic field, which is helpful to increase the SERS activity.[25] For the silver nanostructural arrays in this paper, the number of nanogaps increases with the etching time increasing from 0 to 120 s, which leads to the increase of the density of hot spot. As shown in Figure 2d, the maximal number of nanogaps is obtained in the hybrid nanostructural array of nanocaps and nanotriangles, which is responsible for the highest SERS enhancement. As the etching time increases to 240 s, the nanogaps only locate between the nanorings and nanoparticles, which would decrease the number of nanogaps and the density of hot spots, leading to the weak SERS signals.

The reproducibility of Raman signal is an important parameter for the SERS substrate. Figure 5 shows the SERS spectra of the hybrid array of nanocaps and nanotriangles (etched for 120 s), which are collected from 10 random positions of the substrate. As shown in Figure 5, the standard deviation of the SERS intensity at the band of 1073 cm^{-1} is calculated to be less than 5.0%, indicating the uniformity of the SERS substrate.

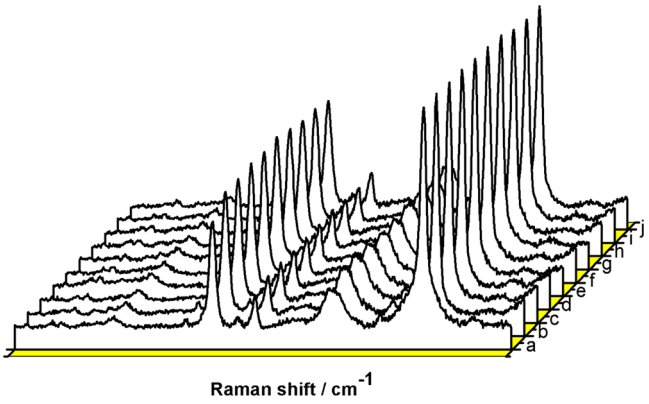

Figure 5. Reproducibility of SERS spectra for the nanocaps and nanotriangles array.

3.3. SERS Enhancement Factor of the Silver Nanostructural Arrays. SERS enhancement factor (EF) is usually used to identify the SERS ability of substrate. The EFs of the arrays of nanocaps, nanocaps and nanotriangles (etched for 120 s), and nanorings and nanoparticles are calculated according to[33−36] $EF = (I_{SERS} \times N_{bulk})/(I_{bulk} \times N_{SERS})$. Herein, $N_{bulk} = \rho A_{laser} h N_A / M$ is the average number of probe molecules which is obtained from the bulk 4-MBA. In our research, the diameter of laser spot (A_{laser}) is 1 μm, the density of 4-MBA powder (ρ) is 1.50 g/cm^3, and the molecular weight (M) is 154.19 g/mol. For the Renishaw micro-Raman spectrometer (532 nm laser line), the penetration depth is about 19 μm (h).[25] N_{SERS} is the adsorbed number of 4-MBA on the SERS-active substrate. $N_{SERS} = N_d A_{laser} A_N / \sigma$, where N_d is the density of the PS colloid spheres. A_N is the half surface area of a PS colloid sphere, and σ is an occupied area of a single 4-MBA adsorbed on the substrate, which is about 0.33 nm^2.[13,34,35] Based on the aforementioned equations, the values of N_{bulk} and N_{SERS} are calculated to be 8.74×10^{10} and 4.76×10^6, respectively. I_{SERS} and I_{bulk} are the SERS intensity of 4-MBA adsorbed on three types of silver nanostructural arrays and the Raman intensity of the bulk 4-MBA, respectively. The values of I_{SERS}/I_{bulk} are 1.54, 10.21, and 3.44, for the arrays of nanocaps, nanocaps and nanotriangles (etched for 120 s), and nanorings and nanoparticles, respectively. Therefore, the values of EF are calculated to be 2.84×10^4, 1.87×10^5, and 6.32×10^4 for the arrays of nanocaps, nanocaps and nanotriangles (etched for 120 s), and nanorings and nanoparticles at the band of 1073 cm^{-1}, respectively, which is shown in Figure 6. The results show that the novel array of nanocaps and nanotriangles has large EF, which is estimated to be seven times larger than that in the array of nanocaps and three times larger than that in the array of nanorings and nanoparticles.

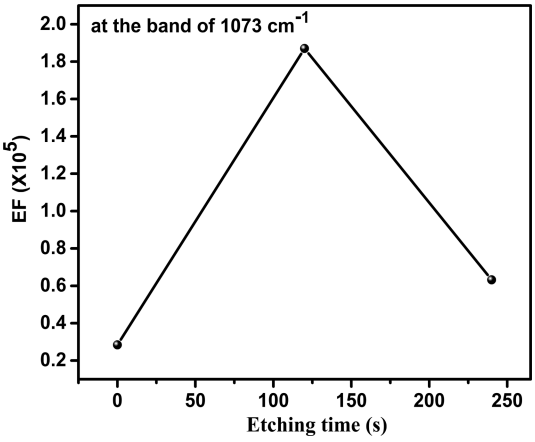

Figure 6. Etching time dependence of SERS enhancement factor for the three nanostructural arrays at the band of 1073 cm^{-1}.

3.4. FDTD Simulations of the Silver Nanostructural Arrays. The FDTD simulation is employed for numerically calculating electromagnetic fields around the silver arrays of nanocaps, nanocaps and nanotriangles (etched for 120 s), and nanorings and nanoparticles to study the effects of different nanostructrual arrays on the hot spots distribution. The simulation results show that the distribution of the hot spots is significantly influenced by different morphology. For the silver nanocaps array, the hot spots are in the regions between the nearest two nanocaps,[37,38] which is shown in Figure 7a. In the silver array of nanocaps and nanotriangles (etched for 120 s), a large number of nanogaps appear, so in this case, the density of hot spots increases remarkably, which can be seen from the top image of Figure 7b. As indicated by the SEM image (Figure 2d), the surface of nanocaps in this nanostructure is very rough, which can affect the distribution of electromagnetic field as well. In the FDTD simulation, this structure is regarded as the nanocaps and nanotriangles covered with some silver nanoparticles. According to the AFM image in Figure 2f, the diameter of silver nanoparticles of the film is estimated to be 25 nm. The simulation data reveals that the electromagnetic field also distributes at the surface of silver nanocaps and nanotriangles,[39−42] which can be clearly observed

DOI: 10.1021/acsami.6b14008
ACS Appl. Mater. Interfaces 2017, 9, 7710−7716

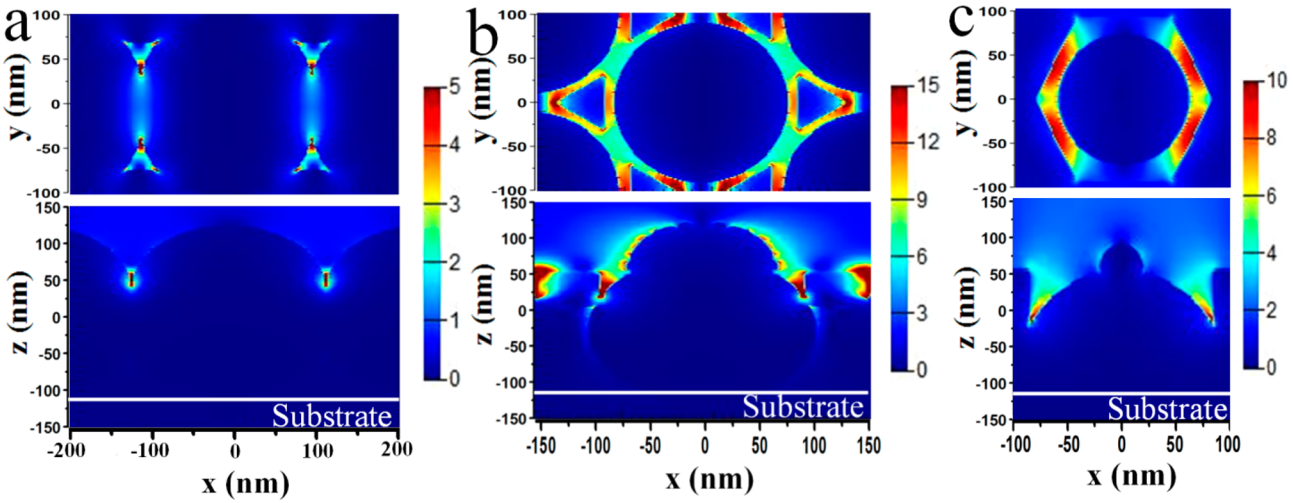

Figure 7. FDTD simulation results for the array of (a) nanocaps, (b) nanocaps and nanotriangles (etched for 120 s), and (c) nanorings and nanoparticles. The top and bottom rows show the electromagnetic fields distribution of top and side views, respectively.

from the bottom image of Figure 7b. Therefore, the hybrid nanocaps and naotriangles array has the highest density of hot spots, which is responsible for the highest enhancement of SERS. As for the silver nanorings and nanoparticles array, the FDTD simulation result demonstrates that the strong electromagnetic field only distributes in the nanogaps between the nanorings and nanoparticles, while the electromagnetic field located on the surface of nanoparticles is very weak, shown in the top and bottom images of Figure 7c. Meanwhile, the number of nanogaps in this array reduces markedly, which leads to the decrease of the density of hot spots and relatively weak SERS signals. Here the FDTD simulation agrees well with the experimental data for the three types of silver nanostructrual arrays, suggesting its feasibility in the simulation of the distribution hot spots.

4. CONCLUSION

In this work, we report an easy-handling and low-cost method to prepare the large-area hybrid nanostructrual arrays with high density of hot spots. By controlling the etching time of PS colloid spheres array in silver nanobowls, three different nanostructural arrays of nanocaps, nanocaps and nanotriangles, and nanorings and nanoparticles are prepared. The strongest SERS signals are observed in the hybrid array of silver nanocaps and nanotriangles (etched for 120 s), for which the EF is estimated to be 1.87×10^5. Experimental results indicate that these SERS signals are reproducible and uniform across the sample surface. The FDTD simulation demonstrates that the large SERS signals stem from the high density of hot spots and enhanced electromagnetic field. This work provides a promising way to prepare the SERS-active substrates with good performance.

AUTHOR INFORMATION

Corresponding Authors

*E-mail: wangdh@nju.edu.cn.
*E-mail: yjzhang@jlnu.edu.cn.

ORCID

Xiaoyu Zhao: 0000-0002-4006-6296

Author Contributions

X.Z. carried out the samples preparation and most of the measurements. X.Z., Y.Z., and D.W. designed the outline of the manuscript and wrote the main manuscript text. All authors contributed to the manuscript with discussion and revision.

Notes

The authors declare no competing financial interest.

ACKNOWLEDGMENTS

This work is supported by the National Natural Science Foundation of China (Nos. 61575080, 61675090, 21676115, and 21546013), Program for the development of Science and Technology of Jilin province (Nos. 20150519024JH, 20150520015JH, 20160101287JC, and 20140519003JH). We would like to thank S. L. Tang, D. Y. Li, and C. X. Lei of Nanjing University for the support of FDTD simulation and valuable discussion.

REFERENCES

(1) Sharma, B.; Frontiera, R. R.; Henry, A. I.; Ringe, E.; Van Duyne, R. P. SERS: Materials, Applications, and the Future. *Mater. Today* **2012**, *15*, 16−25.
(2) Wang, Y. Q.; Yan, B.; Chen, L. X. SERS Tags: Novel Optical Nanoprobes for Bioanalysis. *Chem. Rev.* **2013**, *113*, 1391−1428.
(3) Halas, N. J.; Lal, S.; Chang, W. S.; Link, S.; Nordlander, P. Plasmons in Strongly Coupled Metallic Nanostructures. *Chem. Rev.* **2011**, *111*, 3913−3961.
(4) Stiles, P. L.; Dieringer, J. A.; Shah, N. C.; Van Duyne, R. P. Surface-Enhanced Raman Spectroscopy. *Annu. Rev. Anal. Chem.* **2008**, *1*, 601−626.
(5) Li, J. F.; Huang, Y.; Ding, Y.; Yang, Z. L.; Li, S. B.; Zhou, X. S.; Fan, F. R.; Zhang, W.; Zhou, Z. Y.; Wu, D. Y.; Ren, B.; Wang, Z. L.; Tian, Z. Q. Shell-isolated Nanoparticle-enhanced Raman Spectroscopy. *Nature* **2010**, *464*, 392−395.
(6) Shiohara, A.; Wang, Y. S.; Liz-Marzán, L. M. Recent Approaches toward Creation of Hot Spots for SERS Detection. *J. Photochem. Photobiol., C* **2014**, *21*, 2−25.
(7) Wang, J.; Huang, L. Q.; Zhai, L. P.; Yuan, L.; Zhao, L. H.; Zhang, W. W.; Shan, D. Z.; Hao, A. W.; Feng, X. H.; Zhu, J. Hot Spots Engineering in Hierarchical Silver Nanocap Array for Surface-enhanced Raman Scattering. *Appl. Surf. Sci.* **2012**, *261*, 605−609.
(8) Fan, M. K.; Andrade, G. F. S.; Brolo, A. G. A Review on the Fabrication of Substrates for Surface Enhanced Raman Spectroscopy and their Applications in Analytical Chemistry. *Anal. Chim. Acta* **2011**, *693*, 7−25.

DOI: 10.1021/acsami.6b14008
ACS Appl. Mater. Interfaces 2017, 9, 7710−7716

(9) Polavarapu, L.; Liz-Marzan, L. M. Towards Low-cost Flexible Substrates for Nanoplasmonic Sensing. *Phys. Chem. Chem. Phys.* **2013**, *15*, 5288−5300.
(10) Guerrini, L.; Graham, D. Molecularly-mediated Assemblies of Plasmonic Nanoparticles for Surface-Enhanced Raman Spectroscopy Applications. *Chem. Soc. Rev.* **2012**, *41*, 7085−7107.
(11) Haynes, C. L.; Van Duyne, R. P. Nanosphere Lithography: A Versatile Nanofabrication Tool for Studies of Size-Dependent Nanoparticle Optics. *J. Phys. Chem. B* **2001**, *105*, 5599−5611.
(12) Yan, W. G.; Qi, J. W.; Li, Z. B.; Tian, J. G. Fabrication and Optical Properties of Au-Coated Polystyrene Nanosphere Arrays with Controlled Gaps. *Plasmonics* **2014**, *9*, 565−571.
(13) Lin, W. C.; Liao, L. S.; Chen, Y. H.; Chang, H. C.; Tsai, D. P.; Chiang, H. P. Size Dependence of Nanoparticle-SERS Enhancement from Silver Film over Nanosphere (AgFON) Substrate. *Plasmonics* **2011**, *6*, 201−206.
(14) Greeneltch, N. G.; Blaber, M. G.; Henry, A. I.; Schatz, G. C.; Van Duyne, R. P. Immobilized Nanorod Assemblies: Fabrication and Understanding of Large Area Surface-Enhanced Raman Spectroscopy Substrates. *Anal. Chem.* **2013**, *85*, 2297−2303.
(15) Lin, W. C.; Huang, S. H.; Chen, C. L.; Chen, C. C.; Tsai, D. P.; Chiang, H. P. Controlling SERS Intensity by Tuning the Size and Height of a Silver Nanoparticle Array. *Appl. Phys. A: Mater. Sci. Process.* **2010**, *101*, 185−189.
(16) Zrimsek, A. B.; Henry, A. I.; Van Duyne, R. P. Single Molecule Surface-Enhanced Raman Spectroscopy without Nanogaps. *J. Phys. Chem. Lett.* **2013**, *4*, 3206−3210.
(17) Jensen, T. R.; Malinsky, M. D.; Haynes, C. L.; Van Duyne, R. P. Nanosphere Lithography: Tunable Localized Surface Plasmon Resonance Spectra of Silver NanoparticlesJ. *J. Phys. Chem. B* **2000**, *104*, 10549−10556.
(18) Tian, S.; Zhou, Q.; Gu, Z. M.; Gu, X. F.; Zheng, J. W. Fabrication of a Bowl-shaped Silver Cavity Substrate for SERS-based Immunoassay. *Analyst* **2013**, *138*, 2604−2612.
(19) Chen, X.; Wei, X.; Jiang, K. Large-scale Fabrication of Ordered Metallic Hybrid Nanostructures. *Opt. Express* **2008**, *16*, 11888−11893.
(20) Ho, C. C.; Zhao, K.; Lee, T. Y. Quasi-3D Gold Nanoring Cavity Arrays with High-density Hot-spots for SERS Applications via Nanosphere Lithography. *Nanoscale* **2014**, *6*, 8606−8611.
(21) Coutts, M. J.; Zareie, H. M.; Cortie, M. B.; Phillips, M. R.; Wuhrer, R.; McDonagh, A. M. Exploiting Zinc Oxide Re-emission to Fabricate Periodic Arrays. *ACS Appl. Mater. Interfaces* **2010**, *2*, 1774−1779.
(22) Li, Y.; Cai, W. P.; Duan, G. T. Ordered Micro/Nanostructured Arrays Based on the Monolayer Colloidal Crystals. *Chem. Mater.* **2008**, *20*, 615−624.
(23) Camden, J. P.; Dieringer, J. A.; Zhao, J.; Van Duyne, R. P. Controlled Plasmonic Nanostructures for Surface-Enhanced Spectroscopy and Sensing. *Acc. Chem. Res.* **2008**, *41*, 1653−1661.
(24) He, X.; Yue, C.; Zang, Y. S.; Yin, J.; Sun, S. B.; Li, J.; Kang, J. Y. Multi-hot Spot Configuration on Urchin-like Ag Nanoparticle/ZnO Hollow Nanosphere Arrays for Highly Sensitive SERS. *J. Mater. Chem. A* **2013**, *1*, 15010−15015.
(25) Wang, Y. X.; Zhao, X. Y.; Chen, L.; Chen, S.; Wei, M. B.; Gao, M.; Zhao, Y.; Wang, C.; Qu, X.; Zhang, Y. J.; Yang, J. H. Ordered Nanocap Array Composed of SiO_2 Isolated Ag Islands as SERS Platform. *Langmuir* **2014**, *30*, 15285−15291.
(26) Wang, Y. X.; Zhao, X. Y.; Li, W.; Liu, Y.; Zhang, Y. J.; Zhang, X. L.; Jiang, Y. H.; Liu, S. S.; Yang, J. H. Controlled Magnetic Behavior of [Co/Pt]n Multilayer by Tuning the Topography of 2D Nanobowl Arrays. *J. Alloys Compd.* **2013**, *578*, 488−492.
(27) Li, D. Y.; Lei, C. X.; Chen, L. Y.; Tang, Z. X.; Zhang, S. Y.; Tang, S. L.; Du, Y. W. Waveguide Plasmon Resonance Induced Enhancement of the Magneto-optics in a Ag/Bi:YIG Bilayer Structure. *J. Opt. Soc. Am. B* **2015**, *32*, 2003−2008.
(28) Saracut, V.; Giloan, M.; Gabor, M.; Astilean, S.; Farcau, C. Polarization-Sensitive Linear Plasmonic Nanostructures via Colloidal Lithography with Uniaxial Colloidal Arrays. *ACS Appl. Mater. Interfaces* **2013**, *5*, 1362−1369.
(29) Orendorff, C. J.; Gole, A.; Sau, T. K.; Murphy, C. J. Surface-Enhanced Raman Spectroscopy of Self-Assembled Monolayers: Sandwich Architecture and Nanoparticle Shape Dependence. *Anal. Chem.* **2005**, *77*, 3261−3266.
(30) Yang, L. B.; Jiang, X.; Ruan, W. D.; Yang, J. X.; Zhao, B.; Xu, W. Q.; Lombardi, J. R. Charge-Transfer-Induced Surface-Enhanced Raman Scattering on Ag-TiO_2 Nanocomposites. *J. Phys. Chem. C* **2009**, *113*, 16226−16231.
(31) Xu, S. P.; Ji, X. H.; Xu, W. Q.; Li, X. L.; Wang, L. Y.; Bai, Y. B.; Zhao, B.; Ozaki, Y. Immunoassay using Probe-labelling Immunogold Nanoparticles with Silver Staining Enhancement via Surface-enhanced Raman Scattering. *Analyst* **2004**, *129*, 63−68.
(32) Jiang, X.; Li, X. L.; Jia, X. F.; Li, G. Z.; Wang, X.; Wang, G. Y.; Li, Z. S.; Yang, L. B.; Zhao, B. Surface-Enhanced Raman Scattering from Synergistic Contribution of Metal and Semiconductor in TiO_2/MBA/Ag(Au) and Ag(Au)/MBA/TiO_2 Assemblies. *J. Phys. Chem. C* **2012**, *116*, 14650−14655.
(33) Zhang, M. F.; Zhao, A. W.; Sun, H. H.; Guo, H. Y.; Wang, D. P.; Li, D.; Gan, Z. B.; Tao, W. Y. Rapid, Large-scale, Sonochemical Synthesis of 3D Nanotextured Silver Microflowers as Highly Efficient SERS Substrates. *J. Mater. Chem.* **2011**, *21*, 18817−18824.
(34) Orendorff, C. J.; Gole, A.; Sau, T. K.; Murphy, C. J. Surface-Enhanced Raman Spectroscopy of Self-Assembled Monolayers: Sandwich Architecture and Nanoparticle Shape Dependence. *Anal. Chem.* **2005**, *77*, 3261−3266.
(35) Xia, L. X.; Jia, Y.; Liu, G. Y.; Yang, Z. L.; Chen, X. W.; Zhang, H. L.; Sun, M. T. Adjustment and Control of SERS Activity of Metal Substrates by Pressure. *J. Raman Spectrosc.* **2009**, *41*, 398−405.
(36) Lee, S. H.; Bantz, K. C.; Lindquist, N. C.; Oh, S. H.; Haynes, C. L. Self-Assembled Plasmonic Nanohole Arrays. *Langmuir* **2009**, *25*, 13685−13693.
(37) Farcau, C.; Astilean, S. Mapping the SERS Efficiency and Hot-Spots Localization on Gold Film over Nanospheres Substrates. *J. Phys. Chem. C* **2010**, *114*, 11717−11722.
(38) Fromm, D. P.; Sundaramurthy, A.; Schuck, P. J.; Kino, G.; Moerner, W. E. Gap-Dependent Optical Coupling of Single "Bowtie" Nanoantennas Resonant in the Visible. *Nano Lett.* **2004**, *4*, 957−961.
(39) Correia-Ledo, D.; Gibson, K. F.; Dhawan, A.; Couture, M.; Vo-Dinh, T.; Graham, D.; Masson, J. F. Assessing the Location of Surface Plasmons Over Nanotriangle and Nanohole Arrays of Different Size and Periodicity. *J. Phys. Chem. C* **2012**, *116*, 6884−6892.
(40) Tabatabaei, M.; Sangar, A.; Kazemi-Zanjani, N.; Torchio, P.; Merlen, A.; Lagugne-Labarthet, F. Optical Properties of Silver and Gold Tetrahedral Nanopyramid Arrays Prepared by Nanosphere Lithography. *J. Phys. Chem. C* **2013**, *117*, 14778−14786.
(41) Stewart, M. E.; Mack, N. H.; Malyarchuk, V.; Soares, J.; Lee, T. W.; Gray, S. K.; Nuzzo, R. G.; Rogers, J. A. Quantitative Multispectral Biosensing and 1D Imaging using Quasi-3D Plasmonic Crystals. *Proc. Natl. Acad. Sci. U. S. A.* **2006**, *103*, 17143−17148.
(42) Su, K.-H.; Wei, Q.-H.; Zhang, X.; Mock, J. J.; Smith, D. R.; Schultz, S. Interparticle Coupling Effects on Plasmon Resonances of Nanogold Particles. *Nano Lett.* **2003**, *3*, 1087−1090.

DOI: 10.1021/acsami.6b14008
ACS Appl. Mater. Interfaces 2017, 9, 7710−7716